

# Parity solitons in nonresonantly driven-dissipative condensate channels

H. Sigurðsson,<sup>1,\*</sup> T.C.H. Liew,<sup>2</sup> and I.A. Shelykh<sup>1,3</sup>

<sup>1</sup>*Science Institute, University of Iceland, Dunhagi-3, IS-107 Reykjavik, Iceland*

<sup>2</sup>*Division of Physics and Applied Physics, School of Physical and Mathematical Sciences, Nanyang Technological University 637371, Singapore*

<sup>3</sup>*ITMO University, St. Petersburg 197101, Russia*

(Dated: December 14, 2024)

We study analytically and numerically the condensation of a driven-dissipative exciton-polariton system using symmetric nonresonant pumping geometries. We show that the lowest condensation threshold solution carries a definite parity as a consequence of the symmetric excitation profile. At higher pump intensities competition between the two parities can result in critical quenching of one and saturation of the other. Using long pump channels, we show that the competition of the condensate parities gives rise to a new type of topologically stable defect propagating indefinitely along the condensate. The defects display repulsive interactions and are characterized by a sustained wavepacket carrying a pair of opposite parity domain walls in the condensate channel.

A great deal of work has been devoted in understanding the physics of equilibrium condensate systems such as cold atoms and superconductors. Within the mean field theory the nonlinear nature of these quantum fluids is eloquently captured revealing superfluid currents, vortices, and solitons<sup>1</sup>. Solitons are self-supporting wavepackets maintaining their shape and group velocity as a consequence of dispersive and nonlinear terms compensating each other. They have been studied and observed in numerous physical systems such as optical media<sup>2</sup>, proteins<sup>3</sup>, superfluids<sup>4</sup>, Bose-Einstein condensates<sup>5</sup>, and magnetic materials<sup>6</sup>. They can be classified as non-topological or topological, the latter meaning that they belong to a group of different homotopy than the soliton-free state and thus are stable against decay to a topologically trivial field distribution.

One should also discriminate between conservative solitons appearing in the systems described by the nonlinear Schrödinger, Korteweg- de Vries and sine-Gordon equations and dissipative solitons appearing in the systems described by various modifications of the complex Ginzburg- Landau equation. Among the latter one can mention exciton-polariton condensates<sup>7</sup>, optical parametric oscillators<sup>8</sup>, cold atoms<sup>9</sup>, and optically driven Rydberg clusters<sup>10</sup>. In all these cases a dissipative macroscopic quantum state is continuously replenished by external driving. For this, exciton-polaritons are excellent candidates displaying the solid state analog of Bose-Einstein condensation under either optical or electrical driving<sup>7,11–15</sup> for surprisingly high temperatures<sup>16,17</sup>. This opens a way for the potential application of polaritonic systems in design of optoelectronic devices of next generation<sup>18,19</sup>. Indeed, polariton solitons have been considered as candidates for information processing schemes<sup>20</sup>, are compatible with topological polariton systems<sup>21</sup> and their entanglement has been suggested<sup>22</sup>.

Due to strong polariton-polariton interactions polariton condensates also represent a unique laboratory for the simulation of a plethora of nonlinear quantum phenomena. Features of dark and bright solitons, although not shown to stay supported indefinitely, were recently

observed in phase locked polariton condensates<sup>23</sup> and have been predicted in hyperbolic regions of negative effective mass in patterned microcavities<sup>24</sup>. Dark solitons were found to stay supported through the gain-decay mechanism of the polariton condensate with<sup>25</sup> or without<sup>26</sup> trapping but with no evidence as of yet for propagation. The prediction of oblique dark solitons<sup>27</sup> was also verified for polariton fluids<sup>28</sup> followed by the prediction of oblique dark half-solitons in spinor condensates<sup>29</sup> and later their experimental observation<sup>30</sup>. Furthermore, bright solitons have been predicted<sup>31</sup> and observed<sup>32</sup> in polariton fluids.

In this paper, we analyze the gain and dissipation properties of a polariton condensate under nonresonant CW symmetric spatial pumping. In experiment, the use of symmetric pump shapes is a conventional protocol and thus deserves some analytical treatment. We find that in 1D systems the condensation threshold  $P_{\text{cond}}$  is determined by an order parameter of definite parity due to the symmetric nature of the pump gain. We also show that a second critical pump intensity  $P_{\text{crit}}$  exists where the uncondensed parity suddenly condenses and drives the existing parity to zero. This effect can be thought of as a *cross-saturation* between the parities of the system. Extending the 1D system to 2D opens up a new spatial degree of freedom allowing polaritons to travel parallel to the pump. We find that small amplitudes of random noise result in topologically distinct defect states traveling without dissipation in the condensate. The defects are supported by their nontrivial polariton flow and possess a pair of domain walls of opposite parity to the defect free condensate, making them *parity solitons*. They are found to exist over a wide range of pump powers, pump shapes, interaction strengths and even with no pump induced- or external trapping. Our work is the first evidence of a propagating non-dissipative soliton state in nonresonantly driven polariton condensates, an important step towards realizing optoelectronic platforms based on soliton signals.

*Theory*— Spinless driven-dissipative polariton condensates can be accurately modeled using the complex

Ginzburg-Landau equation for the scalar order parameter  $\Psi$ <sup>33–35</sup>.

$$i\dot{\Psi} = \left[ -\frac{\hbar\nabla^2}{2m} + (g_P + i)P(\mathbf{r}) - i\Gamma + (\alpha - iR)|\Psi|^2 \right] \Psi. \quad (1)$$

Here  $P(\mathbf{r})$  is the nonresonant pump profile,  $g_P$  is the exciton reservoir blueshift induced by the pump,  $m$  is the polariton mass,  $\Gamma$  is the polariton decay rate,  $\alpha$  accounts for polariton-polariton interactions, and  $R$  is the condensate saturation rate.

We begin our analysis on a symmetrically excited condensate considering first 1D geometry and setting both interactions ( $\alpha$ ) and reservoir blueshift ( $g_P$ ) to zero. The dynamics of the order parameter is then characterized only by the polariton dispersion and gain-dissipation mechanism in the system:

$$i\dot{\Psi} = \left[ -\frac{\hbar}{2m} \frac{\partial^2}{\partial x^2} + i(P(x) - \Gamma - R|\Psi|^2) \right] \Psi. \quad (2)$$

Here we set  $P(x) = P(-x)$  and define the intensity of the pump as  $P_0$  where  $P(x) = P_0 p(x)$ . By slowly ramping the pump intensity polaritons condense into a solution with the lowest threshold at a critical value  $P_0 = P_{\text{cond}}$ . Since the condensate decays quickly to zero as polaritons move away from the pump we can choose the infinite quantum well basis with boundaries  $x = \pm L/2$  chosen far away from the condensate in order to extract the parity dependent behavior of the condensate,

$$\Psi = \sum_n A_n \psi_n, \quad n = 0, 1, 2, \dots \quad (3)$$

Plugging Eq. 3 into Eq. 2 and integrating over the spatial component  $x$  we get:

$$\begin{aligned} \dot{A}_n = & -(i\omega_n + \Gamma) A_n + P_0 \sum_m p_{nm} A_m \\ & + R \sum_{jkl} M_{njkl} A_j^* A_k A_l. \end{aligned} \quad (4)$$

Here  $\hbar\omega_n$  are the energies of the eigenstates  $\psi_n$ . The pump elements  $p_{nm}$  are written as:

$$p_{nm} = \int_{-L/2}^{L/2} P(x) \psi_n \psi_m dx, \quad (5)$$

This integral is nonzero only when the product  $\psi_n \psi_m$  is even. The nonlinear elements are written as:

$$M_{ijkl} = \int_{-L/2}^{L/2} \psi_i \psi_j \psi_k \psi_l dx. \quad (6)$$

This integral has a straightforward analytical solution given our choice of basis (see Sec. B). Defining  $n_n \equiv |A_n|^2$  and looking at the rate of the modes in the linear regime ( $|\Psi|^2 \sim 0$ ) we have,

$$\frac{\dot{n}_n}{2} = P_0 \sum_m p_{nm} \sqrt{n_n n_m} \cos(\phi_n - \phi_m) - \Gamma n_n, \quad (7)$$

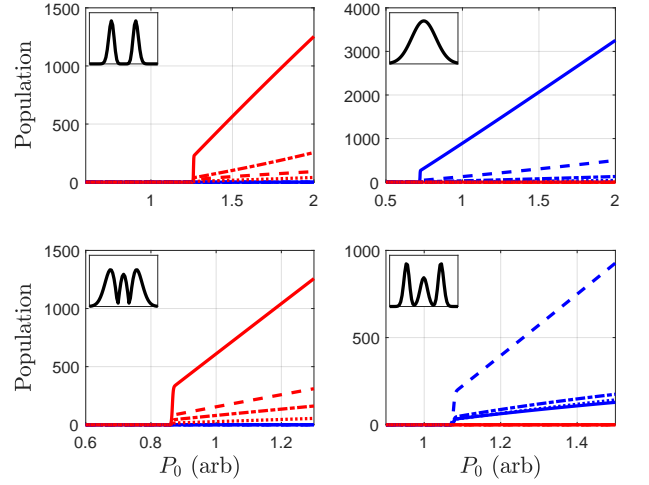


Figure 1. (Color online) Threshold results for a 1D condensate driven by a symmetric pump profile  $p(x)$  (see inset in each panel). Different blue lines correspond to the occupation of even parity eigenstates whereas red lines to odd parity eigenstates.

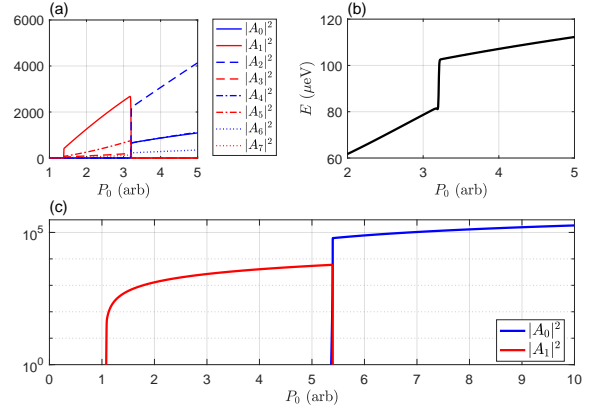


Figure 2. (Color online) (a) Mode population and (b) condensate energy as a function of pump power for 1D system showing the parity switch. (c) Eqs. 9-10 propagated with increasing pump power with  $\omega_0 = \omega_1 = 0$ . Element values were set to  $M_{0000} = 0.001 \mu\text{m}^{-1}$ ,  $M_{1111} = 0.0573 \mu\text{m}^{-1}$ ,  $M_{0011} = 0.01 \mu\text{m}^{-1}$ ,  $p_{00} = 0.032$ ,  $p_{11} = 0.095$ ,  $R = 0.0012 \text{ps}^{-1} \mu\text{m}$ , and  $\Gamma = 0.1 \text{ps}^{-1}$ . Eqs. 13-14 give  $P_{\text{cond}} = 1.05 \text{ps}^{-1}$  and  $P_{\text{crit}} = 5.3 \text{ps}^{-1}$  in good agreement with numerical results.

where  $\phi_n$  is the phase of  $A_n$ . It is now clear that the maximum gain of the system (lowest threshold) is determined by a superposition of same parity modes coupled through  $p_{nm}$ . Thus the lowest threshold condensate solution has definite parity. This is in agreement with observed numerical results where  $P_0$  in Eq. 2 is adiabatically ramped for four different pump profiles (see Fig. 1).

As pump intensity is increased, we observe a second critical pump power where the condensate suddenly flips its parity followed by abrupt shift in energy (see Fig. 2a,b). The effect demonstrates the presence of a sec-

ond condensate solution of the opposite parity, for which the occupation rate changes from negative to positive and which in return quenches the first solution. This scenario becomes clear if one uses a truncated basis of linear eigenstates,

$$\Psi = A_0\psi_0 + A_1\psi_1. \quad (8)$$

which results in the following coupled equations:

$$\frac{\dot{A}_0}{A_0} = -(i\omega_0 + \Gamma) + P_0 p_{00} - R[M_{0000}|A_0|^2 + 2M_{0011}|A_1|^2 + M_{0011}A_1^2 e^{-i2\phi_0}], \quad (9)$$

$$\frac{\dot{A}_1}{A_1} = -(i\omega_1 + \Gamma) + P_0 p_{11} - R[M_{1111}|A_1|^2 + 2M_{0011}|A_0|^2 + M_{0011}A_0^2 e^{-i2\phi_1}]. \quad (10)$$

The rate equations then become,

$$\frac{1}{2} \frac{\dot{n}_0}{n_0} = -\Gamma + P_0 p_{00} - R[M_{0000}n_0 + M_{0011}n_1(2 - \cos(2\phi))], \quad (11)$$

$$\frac{1}{2} \frac{\dot{n}_1}{n_1} = -\Gamma + P_0 p_{11} - R[M_{1111}n_1 + M_{0011}n_0(2 + \cos(2\phi))], \quad (12)$$

where  $\phi = \phi_2 - \phi_1$ . The lowest condensation threshold is then determined by,

$$P_{\text{cond}} = \min \left\{ \frac{\Gamma}{p_{00}}, \frac{\Gamma}{p_{11}} \right\}. \quad (13)$$

Let us assume that  $P_{\text{cond}} = \Gamma/p_{11}$  is minimal. Then the  $A_1$  mode condenses first and has a steady state according to  $n_1 = (P_0 p_{11} - \Gamma)/R M_{1111}$ . Eqs. 11-12 show that cross-saturation effects are tunable through the phase difference between the two modes. Without any loss of generality we can set  $\omega_0 = \omega_1 = 0$  which restricts the phase to  $\phi = n\pi/2$  where  $n \in \mathbb{Z}$ . It becomes then obvious that  $\phi = 0$  creates the optimum condition for the  $A_0$  mode to become populated since it minimizes the saturation caused by the  $A_1$  mode. The critical pump power where the rate of the  $A_0$  mode turns positive is then,

$$P_{\text{crit}} = \Gamma \frac{1 - M_{0011}/M_{1111}}{p_{00} - M_{0011}p_{11}/M_{1111}}. \quad (14)$$

It is clear that in order for the modes to switch then  $P_{\text{crit}} > P_{\text{cond}}$ . The quenching of the existing mode then corresponds to a class of solutions determined by the elements  $p_{nm}$  and  $M_{ijkl}$  where  $P_0 \geq P_{\text{crit}}$  causes the rate of the previously dominant mode to become strictly negative, driving it to zero. In Fig. 2c we show the parity flip for Eqs. 9-10 for an arbitrary set of pump and nonlinear elements in good agreement with Eqs 13-14. We explicitly synchronized the energies in order to emphasize that the effect can purely be explained via the gain-decay mechanism. We note that the effect does not vanish for

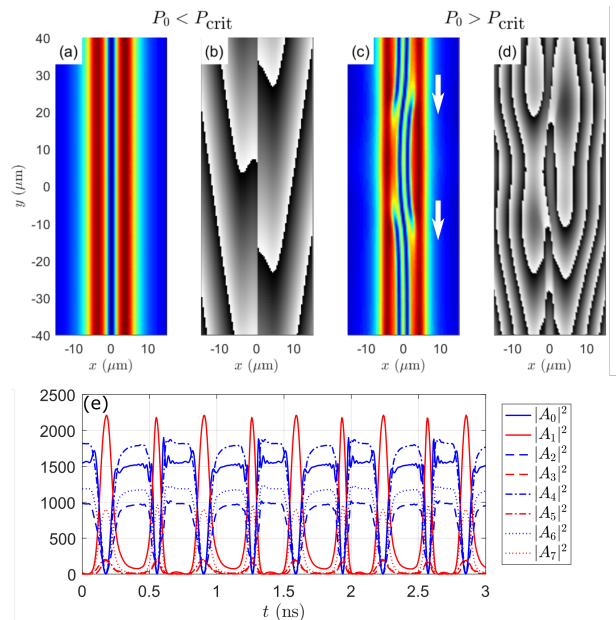


Figure 3. (Color online) Density (a) and phase (b) of the condensate in an odd parity solution with  $k_y \neq 0$  with  $P_0 = 1 \text{ ps}^{-1}$ . (c,d) The same channel after driving the pump intensity past  $P_{\text{crit}}$ . Background noise and finite  $k_y$  wavevectors result in the formation of defects traveling along the channel indefinitely (white arrows). Here  $P_0 = 3.5 \text{ ps}^{-1}$ . (e) Mode population at  $y = 0$  from panels (c,d). The even parity (blue lines) of the channel drops to zero when the odd parity defects travel past  $y = 0$ . The two defects travel at a fixed velocity, with a fixed parity and without decaying.

nonzero real interactions  $\alpha$  and/or additional confining potentials  $V(x)$ .

In the case of an asymmetric pump profile the pump elements  $p_{nm}$  mix together the gain of the two parities. In Sec. C we investigate the effect such asymmetry and find that at critical skewing strength the parity switch is replaced by a solution of mixed modes resulting in an asymmetric condensate. The presence of noise in the pump is also investigated and is found to have a small effect on the parity switch.

*Parity Solitons* — We now return to Eq. 1 where  $\alpha \neq 0$  and  $g_P \neq 0$ . Considering the realistic case of 2D polaritons we chose the pump profile from Fig. 1a in the form of a channel along the  $y$ -axis. The same results as for 1D systems are observed if the order parameter possesses zero longitudinal wavevectors ( $k_y = 0$ ). In the case of non-zero longitudinal wavevectors (see Fig. 3a,b) the parity switch threshold ( $P_{\text{crit}}$ ) with weak stochastic noise can result in the formation of localized defect states traveling along the channel carrying opposite parity charges (see Fig. 3c,d,e). The phase pattern of the defects makes them topologically distinct from the defect-free solution and thus they can be classified as topologically stable. Since the parity switch is a continuous transition we observe that the number of defects appearing in the channel is proportional to the pump ramp rate. In the case of adi-

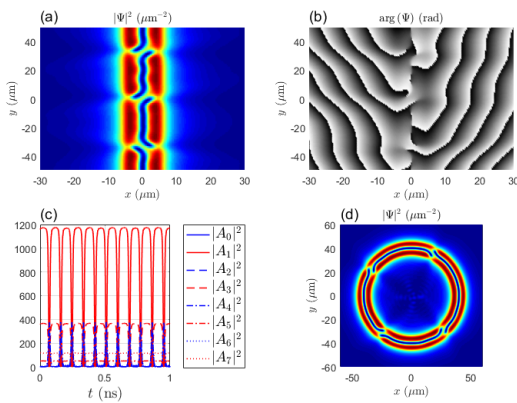


Figure 4. (Color online) Condensate (a) density and (b) phase with three defect states after instantaneous switching of the pump at  $P_0 = 1 \text{ ps}^{-1}$ . (c) Mode population at  $y = 0$ . In the final state the defects are equidistant from each other and travel along the channel showing regular oscillations in the parity at  $y = 0$ . (d) Defects traveling along a circular pump profile.

abatic increasing of pump intensity ( $dP_0/dt \rightarrow 0$ ) no defects are observed. Parameter values are set to  $\alpha = 0.003 \text{ ps}^{-1} \mu\text{m}^2$ ,  $R = 0.3\alpha$ ,  $\Gamma = 0.1 \text{ ps}^{-1}$ ,  $m = 7 \times 10^{-5} m_0$ ,  $g_P = 3\alpha$ , where  $m_0$  is the free electron rest mass.

The defects do not only form around  $P_{\text{crit}}$ . Instantaneous switching of the pump and subsequent condensation of the polaritons is a transition from a linear state to a saturated state which can give birth to defects seeded by random noise. Nonresonant pulsing of the defect free channel can also induce their formation. In Fig. 4a,b we show the final state after instantaneous switching of the pump where three defects travel in unison along the channel. Differently from Fig. 3 where the channel is of even parity with odd parity defects, here the channel is of odd parity with even parity defects. This result underlines that the defects can exist in either parity opposite of the channel. We observe defect formation at pump values where only one channel solution is stable verifying that the origin of the defects is not due to the bistability between the channel solutions<sup>37</sup>. The defects are found to possess repulsive interactions and are unable to pass through each other. Instead, they display damped oscillatory behavior until maximum separation is achieved between the defects where they either become static or move in unison along the channel. If the channel ends are open then the defects escape and dissipate from the system. In order to capture the defects in experiment, a circular channel can be used (see Fig. 4d). In Fig. 5 we plot the velocity field (black arrows) and density (colormap) of the polaritons for the two different defect types. In Fig. 5a we observe two in-phase sources of flux and two vortical points (white crosses) causing polaritons to flow freely across the channel. In Fig. 5b we find two sources of flux  $\pi$  out-of-phase and a single saddle point in the center of the channel. We note that the defect in Fig. 5b

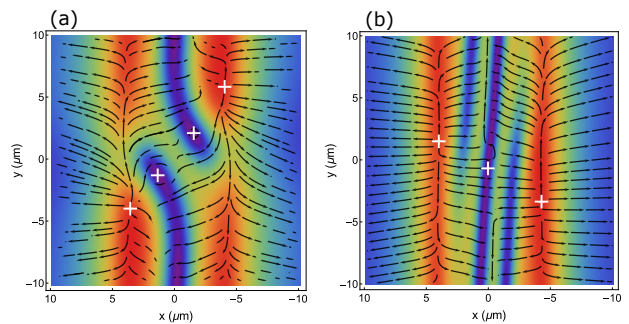


Figure 5. (Color online) Velocity streamlines (black arrows) and density of the polariton condensate for an (a) even parity defect and (b) odd parity defect in the channel. White crosses denote sources of flux, circulation, and saddle points.

can be regarded as a type of *dark soliton* due to the density minimum gashing diagonally across the channel. In Fig. 5a the defects are reminiscent of *bright solitons* since a finite density connects across the channel. This raises the question whether the same defects can exist for attractive interactions ( $\alpha < 0$ ). Indeed, the defects can be regarded as 1D solutions of the pump trapped within the channel making them solitonic.

We determine that the defects can exist over a wide range of interaction strength  $\alpha \in [0.4, 3.5]\alpha_0$  and pump blueshift  $g_P \in [0, 17]g_{P0}$  where  $\alpha_0 = 0.003 \text{ ps}^{-1} \mu\text{m}^2$  and  $g_{P0} = 3\alpha_0$ . Here the parameter ranges were determined from propagating a single defect while slowly increasing or decreasing the value of  $g_P$  or  $\alpha$ . We note that the existence of the defects for  $g_P = 0$  highlights that they are artifacts of nonlinearity rather than trapping. For increased values of  $\alpha$  modulations appear in the condensate density indicating instability in the stationary uniform channel. The defect survives until the modulations become larger than its characteristic size where it breaks up. Other pump intensities/profiles will have their own range of allowed blueshifts and interactions which is a subject for future investigation.

Lastly, we investigated the propagation of the defects in the presence of static disorder<sup>38</sup>. Depending on the disorder landscape the defects can either pass unhindered along the channel, become trapped between disorder maxima, or break up. To our surprise, we find that a defect trapped in the potential landscape oscillates without damping as opposed to damped collisions with other defects (see supplemental animation).

*Conclusions* — We've analyzed analytically and numerically the effects of symmetric nonresonant pumping in polariton condensates in 1D systems. We show that the minimum condensation threshold belongs to a condensate of definite parity. We also show the existence of a second critical pump power where the phase degree of freedom allows the opposite parity solution to take up the gain and drive the other parity to zero. Stretching such symmetric pump profiles to form channels in 2D system allows the formation of solitonic parity-defects. The

defects exist over wide range of parameter values including no external- or pump-induced trapping. The defects possess nontrivial velocity patterns making them topologically distinct, and display damped collisions when approaching one another. Different from previously observed solitonic features in polariton condensates, our states travel persistently along the pump channels and do not decay even with constant dissipation present in the system.

*Acknowledgements* — H.S. and I.S. acknowledge support by the Research Fund of the University of Iceland, The Icelandic Research Fund, Grant No. 163082-051. T.L. was supported by the Singaporean MOE grants 2015-T2-1-055 and 2016-T1-1-084. I.A.S. acknowledges support from a mega-grant № 14.Y26.31.0015 and GOSZADANIE № 3.2614.2017 of the Ministry of Education and Science of Russian Federation.

## Appendix A: Extension to a reservoir model

The transition from one parity to another is not exclusive to Eq. 2 in the main text which assumes a static gain at all times. An alternative model takes account of a reservoir  $n_R$  of hot excitons governed by a rate equation,

$$i\dot{\Psi} = \left[ -\frac{\hbar}{2m} \frac{\partial^2}{\partial x^2} + \frac{i}{2} (Rn_R - \Gamma) \right] \Psi, \quad (\text{A1})$$

$$\dot{n}_R = -(\Gamma_R + R|\Psi|^2)n_R + P(\mathbf{r}). \quad (\text{A2})$$

Here  $\Gamma_R$  is the reservoir dissipation rate and  $R$  now plays the role of in-scattering rate from the reservoir to the condensate. We note that under the current consideration the effective potential from interactions with polaritons and the reservoir are set to zero. The reservoir steady state is given by,

$$n_R^{(0)} = \frac{P(\mathbf{r})}{\Gamma_R + R|\Psi^{(0)}|^2}, \quad (\text{A3})$$

where  $|\Psi^{(0)}|^2$  is the condensate steady state density. This more complicated expression of the polariton gain mixes the parities of the system and the matrix elements  $p_{nm}$  from Eq. 5 no longer vanish for  $n$  and  $m$  of different parities. A good choice of a pump profile  $p(x)$  can however reproduce the switch in parities (see Fig. 6) underlining that the transition can still be observed in models of one or more reservoirs.

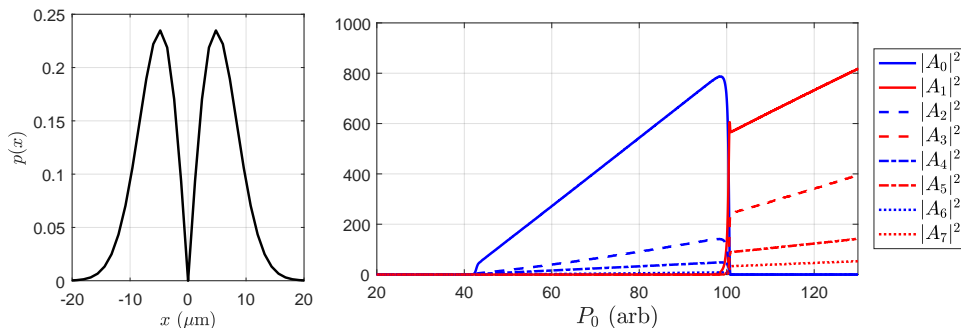


Figure 6. (Color online) (a) Choice of pump profile producing the parity switch using Eq. A1. (b) Population of the first eight linear basis eigenstates.

## Appendix B: Nonlinear matrix elements

The eigenstates of the symmetric infinite quantum well are written,

$$\psi_n = \sqrt{\frac{2}{L}} \sin\left(\frac{(n+1)\pi x}{L}\right), \quad n = 0, 1, 2, \dots \quad (\text{B1})$$

The solution to Eq. 6 in the main text becomes then,

$$M_{nmkq} = \frac{L}{4\pi} \left[ \begin{aligned} & \frac{\sin\left(\frac{1}{2}\pi(k-m-n-q)\right)}{(-k+m+n+q)} + \frac{\sin\left(\frac{1}{2}\pi(k+m-n-q)\right)}{(k+m-n-q)} + \frac{\sin\left(\frac{1}{2}\pi(k-m+n-q)\right)}{(k-m+n-q)} \\ & - \frac{\sin\left(\frac{1}{2}\pi(k+m+n-q)\right)}{(k+m+n-q)} + \frac{\sin\left(\frac{1}{2}\pi(k-m-n+q)\right)}{(k-m-n+q)} - \frac{\sin\left(\frac{1}{2}\pi(k+m-n+q)\right)}{(k+m-n+q)} \\ & - \frac{\sin\left(\frac{1}{2}\pi(k-m+n+q)\right)}{(k-m+n+q)} + \frac{\sin\left(\frac{1}{2}\pi(k+m+n+q)\right)}{(k+m+n+q)} \end{aligned} \right]. \quad (\text{B2})$$

### Appendix C: Effects of noise and asymmetry in the driving field

All results presented are done using a stochastic low amplitude initial condition and background noise added to the order parameter at timesteps much smaller than the characteristic polariton timescales. The noise serves as a method of breaking system symmetries and giving rise to nontrivial states at critical transition points such as condensation ( $P_{\text{cond}}$ ) and parity switching ( $P_{\text{crit}}$ ).

We now investigate additional Gaussian distributed noise field with zero mean added to the pump profile  $p(x)$  at small time steps.

$$p(x)dt = (p_0(x) + \delta(t))dt. \quad (\text{C1})$$

This tests the sensitivity of the parity dependent nature of the gain-decay mechanism. Fig. 7a shows the parity switching taking place undeterred by the static noise distribution (Fig. 7b) added to the pump profile (Fig. 7b).

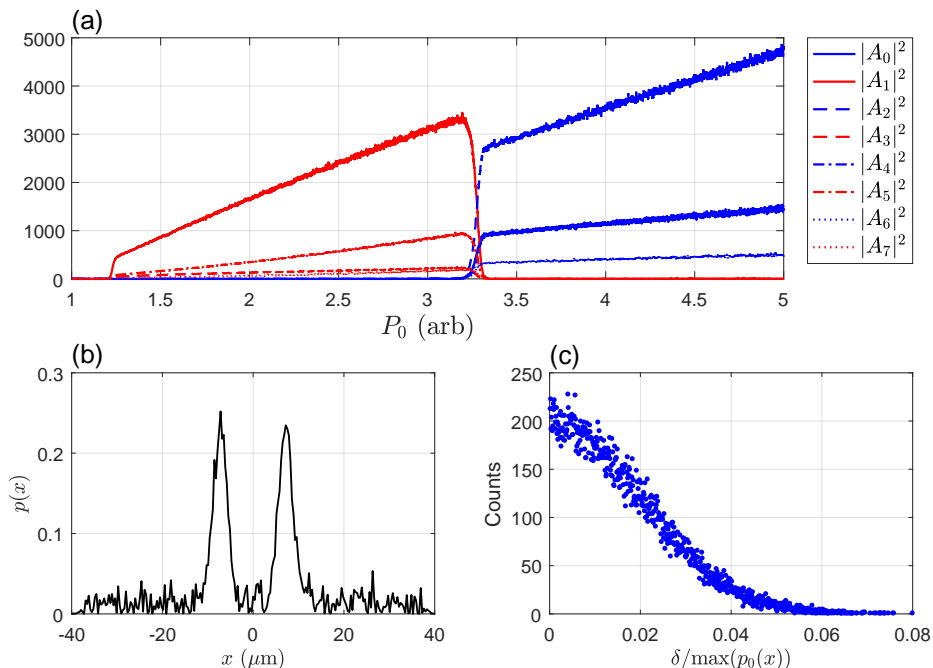


Figure 7. (Color online) (a) Population of the first eight linear basis eigenstates showing a change in parity analogous to Fig. 2a in the main text. (b) Snapshot of the pump profile with added noise. (c) Distribution of the noise.

We next check static asymmetry in the pump profile. Results in Fig. 8 show that asymmetric profiles alters the evolution of the condensate as a function of pump power  $P_0$ . The transition takes place over a larger interval of pump powers due to the pump now mixing different parity eigenstates. Regardless, the for reasonable skewing of the pump profile (Fig. 8a) the parity transition still takes place where a new solution becomes dominant and quenches the other (Fig. 8b). The results underline that the physics at play are robust against reasonable amounts of noise and skewing which can be expected in experiments. We note that here we have only investigated one type of a pump profile whereas other profiles with a different set of pump elements  $p_{nm}$  might be less affected by asymmetry.

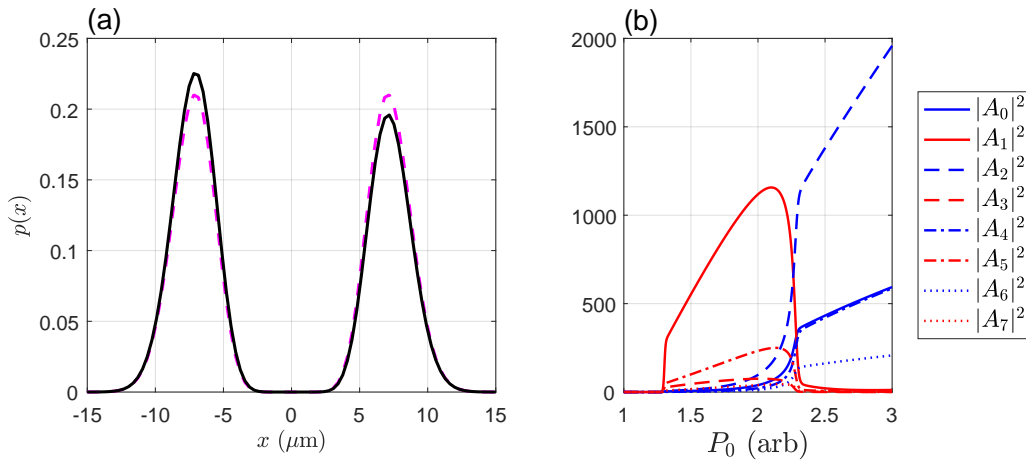


Figure 8. (Color online) (a) Skewed (black solid line) vs symmetric (dashed magenta line) pump profile. (b) Population of the first eight linear basis eigenstates showing a gradual change in parity for the asymmetric pump profile in panel (a).

- 
- \* correspondence address: [helg@hi.is](mailto:helg@hi.is)
- <sup>1</sup> L. Pitaevskii and S. Stringari, *Bose-Einstein Condensation*, International Series of Monographs on Physics (Clarendon Press, 2003).
  - <sup>2</sup> Y. S. Kivshar, G. P. Agrawal, and G. P. Agrawal, *Optical Solitons* (Academic Press, Burlington, 2003).
  - <sup>3</sup> A. Davydov, *Solitons in Molecular Systems*, Mathematics and its applications (D. Reidel Publishing Company): Soviet series (Springer Netherlands, 1985).
  - <sup>4</sup> K. Maki, “Solitons and related phenomena in superfluid  $^3\text{He}$ ,” in *Quantum Fluids and Solids*, edited by S. B. Trickey, E. D. Adams, and J. W. Dufty (Springer US, Boston, MA, 1977) pp. 65–84.
  - <sup>5</sup> C. Becker, S. Stellmer, P. Soltan-Panahi, S. Dorscher, M. Baumert, E.-M. Richter, J. Kronjäger, K. Bongs, and K. Sengstock, *Nat Phys* **4**, 496 (2008).
  - <sup>6</sup> A. M. Kosevich, V. V. Gann, A. I. Zhukov, and V. P. Voronov, *Journal of Experimental and Theoretical Physics* **87**, 401 (1998).
  - <sup>7</sup> I. Carusotto and C. Ciuti, *Rev. Mod. Phys.* **85**, 299 (2013).
  - <sup>8</sup> A. Marandi, Z. Wang, K. Takata, R. L. Byer, and Y. Yamamoto, *Nat Photon* **8**, 937 (2014), letter.
  - <sup>9</sup> H. Ritsch, P. Domokos, F. Brennecke, and T. Esslinger, *Rev. Mod. Phys.* **85**, 553 (2013).
  - <sup>10</sup> M. Saffman, T. G. Walker, and K. Mølmer, *Rev. Mod. Phys.* **82**, 2313 (2010).
  - <sup>11</sup> J. Kasprzak, M. Richard, S. Kundermann, A. Baas, P. Jeambrun, J. M. J. Keeling, F. M. Marchetti, M. H. Szymańska, R. André, J. L. Staehli, *et al.*, *Nature* **443**, 409 (2006).
  - <sup>12</sup> R. Balili, V. Hartwell, D. Snoko, L. Pfeiffer, and K. West, *Science* **316**, 1007 (2007).
  - <sup>13</sup> C. W. Lai, N. Y. Kim, S. Utsunomiya, G. Roumpou, H. Deng, M. D. Fraser, T. Byrnes, P. Recher, N. Kumada, T. Fujisawa, and Y. Yamamoto, *Nature* **450**, 529 (2007).
  - <sup>14</sup> C. Schneider, A. Rahimi-Iman, N. Y. Kim, J. Fischer, I. G. Savenko, M. Amthor, M. Lerner, A. Wolf, L. Worschech, V. D. Kulakovskii, I. A. Shelykh, M. Kamp, S. Reitzenstein, A. Forchel, Y. Yamamoto, and S. Hofling, *Nature* **497**, 348 (2013), letter.
  - <sup>15</sup> T. Byrnes, N. Y. Kim, and Y. Yamamoto, *Nat Phys* **10**, 803 (2014), review.
  - <sup>16</sup> G. Malpuech, A. D. Carlo, A. Kavokin, J. J. Baumberg, M. Zamfirescu, and P. Lugli, *Applied Physics Letters* **81**, 412 (2002).
  - <sup>17</sup> S. Christopoulos, G. B. H. von Högersthal, A. J. D. Grundy, P. G. Lagoudakis, A. V. Kavokin, J. J. Baumberg, G. Christmann, R. Butté, E. Feltin, J.-F. Carlin, and N. Grandjean, *Phys. Rev. Lett.* **98**, 126405 (2007).
  - <sup>18</sup> M. D. Fraser, S. Hofling, and Y. Yamamoto, *Nat Mater* **15**, 1049 (2016), commentary.
  - <sup>19</sup> D. Sanvitto and S. Kena-Cohen, *Nat Mater* **15**, 1061 (2016), review.
  - <sup>20</sup> E. Cancellieri, J. K. Chana, M. Sich, D. N. Krizhanovskii, M. S. Skolnick, and D. M. Whittaker, *Phys. Rev. B* **92**, 174528 (2015).
  - <sup>21</sup> Y. V. Kartashov and D. V. Skryabin, *Optica* **3**, 1228 (2016).
  - <sup>22</sup> W. L. Zhang and S. F. Yu, *Opt. Express* **18**, 21219 (2010).
  - <sup>23</sup> G. Christmann, G. Tosi, N. G. Berloff, P. Tsotsis, P. S. Eldridge, Z. Hatzopoulos, P. G. Savvidis, and J. J. Baumberg, *New Journal of Physics* **16**, 103039 (2014).
  - <sup>24</sup> K. B. Arnardottir, I. V. Iorsh, T. C. Liew, and I. A. Shelykh, *ACS Photonics* (2017), [doi.org/10.1021/acsp Photonics.7b00040](https://doi.org/10.1021/acsp Photonics.7b00040).
  - <sup>25</sup> E. A. Ostrovskaya, J. Abdullaev, M. D. Fraser, A. S. Desyatnikov, and Y. S. Kivshar, *Phys. Rev. Lett.* **110**, 170407 (2013).
  - <sup>26</sup> E. A. Ostrovskaya, J. Abdullaev, A. S. Desyatnikov, M. D. Fraser, and Y. S. Kivshar, *Phys. Rev. A* **86**, 013636 (2012).
  - <sup>27</sup> G. A. El, A. Gammal, and A. M. Kamchatnov, *Phys. Rev. Lett.* **97**, 180405 (2006).
  - <sup>28</sup> A. Amo, S. Pigeon, D. Sanvitto, V. G. Sala, R. Hivet, I. Carusotto, F. Pisanello, G. Leménager, R. Houdré,

- E. Giacobino, C. Ciuti, and A. Bramati, *Science* **332**, 1167 (2011).
- <sup>29</sup> H. Flayac, D. D. Solnyshkov, and G. Malpuech, *Phys. Rev. B* **83**, 193305 (2011).
- <sup>30</sup> R. Hivet, H. Flayac, D. D. Solnyshkov, D. Tanese, T. Boulier, D. Andreoli, E. Giacobino, J. Bloch, A. Bramati, G. Malpuech, and A. Amo, *Nat Phys* **8**, 724 (2012).
- <sup>31</sup> O. A. Egorov, D. V. Skryabin, A. V. Yulin, and F. Lederer, *Phys. Rev. Lett.* **102**, 153904 (2009).
- <sup>32</sup> M. K., N. S. S., G. V., HartleyR., S. V., C.-M. A., BiermannK., HeyR., and S. V., *Nat Photon* **6**, 50 (2012).
- <sup>33</sup> J. Keeling and N. G. Berloff, *Phys. Rev. Lett.* **100**, 250401 (2008).
- <sup>34</sup> M. Wouters and I. Carusotto, *Phys. Rev. Lett.* **99**, 140402 (2007).
- <sup>35</sup> M. Wouters, T. C. H. Liew, and V. Savona, *Phys. Rev. B* **82**, 245315 (2010).
- <sup>36</sup> *See Supplemental Material.*
- <sup>37</sup> H. Sigurdsson, I. A. Shelykh, and T. C. H. Liew, *Phys. Rev. B* **92**, 195409 (2015).
- <sup>38</sup> V. Savona and W. Langbein, *Phys. Rev. B* **74**, 075311 (2006).